Electronic structure and electron transport properties of calcium-zinc amorphous alloys and several intermetallic compounds

1990 J. Phys.: Condens. Matter 2 7825

(http://iopscience.iop.org/0953-8984/2/38/008)

J. Phys.: Condens. Matter **2** (1990) 7825–7839. Printed in the UK

Electronic structure and electron transport properties of calcium–zinc amorphous alloys and several intermetallic compounds

U Mizutani†, T Shimizu†, T Fukunaga†, T Koyano†, K Tanaka‡, M Yamada‡ and T Matsuda§

† Department of Crystalline Materials Science, Nagoya University, Nagoya 464-01, Japan
‡ Department of Materials Science and Engineering, Nagoya Institute of Technology, Nagoya 466, Japan
§ Department of Physics, Aichi University of Education, Kariya-shi, Aichi-ken, 448 Japan

Received 15 January 1990, in final form 18 April 1990

Abstract. The electronic structure and the electron transport properties of the Ca_xZn_{100-x} ($x = 45, 50, 64$ and 75) amorphous alloys have been studied through the measurements of x-ray photoemission spectroscopy (XPS), the low-temperature specific heats, the magnetic susceptibility, the electrical resistivity, the Hall coefficient and the thermoelectric power. The XPS spectra and the low-temperature specific heats were also measured for Ca_3Zn, CaZn, $CaZn_2$ and $CaZn_5$ intermetallic compounds. The prepeak was observed in the x-ray diffraction spectrum for the $Ca_{75}Zn_{25}$ amorphous alloy. This was taken as strong support for the realistic atomic structure model proposed by Hafner and Tegze. It is found that the valence band structure deduced from the XPS spectrum and the electronic specific heat coefficient agrees with that derived from the self-consistent band calculations based on the realistic atomic structure. It is concluded that, in spite of the enhancement of the density of states at the Fermi level due to the sizable contribution of the Ca 3d states, the temperature dependence of the resistivity and the Hall coefficient can be explained by assuming that Zn 4p and Ca 4p electrons at the Fermi level are mostly responsible for the electron conduction.

1. Introduction

Ca-based amorphous alloys containing only non-transition metals such as Al and Mg as partner elements have been considered as one of the most interesting targets for the study of the electron transport mechanism in non-magnetic amorphous alloys (Tsai *et al* 1982, Nagel *et al* 1982, Mizutani and Matsuda 1983, Naugle *et al* 1986, Howson *et al* 1988). It is indeed surprising that Ca–Al amorphous alloys possess an unusually large resistivity exceeding 400 $\mu\Omega$ cm whereas the companion glasses Ca–Mg have a small resistivity of only 40 $\mu\Omega$ cm. Studies on the ternary amorphous alloys $Ca_{70}Mg_{30-x}Al_x$ ($0 \leqslant x \leqslant 30$) and $Ca_{60}Mg_{40-x}Al_x$ ($0 \leqslant x \leqslant 40$) revealed that a rapid increase in the resistivity upon substituting Al for Mg accompanies a systematic change in the temperature dependence of the resistivity (Mizutani *et al* 1987a). This behaviour is exactly the same as observed in typical sp-electron amorphous alloys based on noble metals, Mg and Al (Mizutani and

0953-8984/90/387825 + 15 $03.50

Yoshino 1984, Mizutani *et al* 1988a, 1990) and is interpreted in terms of the generalised Faber–Ziman theory except for the high-resistivity regime above about 200 $\mu\Omega$ cm, where the mean free path is limited by an average atomic distance.

In spite of the apparent consistency with the generalised Faber–Ziman theory, one should realise that Ca-based amorphous alloys possess a unique feature, which is envisaged when the resistivity ρ is plotted against the density of states at the Fermi level E_F or the electronic specific heat coefficient γ. The value of ρ for sp-electron amorphous alloys based on Al, Mg and noble metals mentioned above increases rapidly with decreasing γ and constitutes a master curve in the ρ–γ plot (Mizutani *et al* 1990). However, the data for the Ca–Mg–Al ternary alloys do not fall on this master curve; instead, they are displaced consistently towards a higher γ and form a curve almost parallel to it. This means that the carrier density at E_F in Ca-based alloys is always higher than in other sp-electron amorphous alloys at a given resistivity, suggesting that the carriers are less mobile on average in the Ca-based alloys.

The phase diagrams of Ca–Mg and Ca–Al systems are quite similar to each other, possessing in common the Laves phases $CaMg_2$ and $CaAl_2$ but no stable intermetallic phases on the Ca-rich side, where glass formation is possible. In contrast, the phase diagram of the Ca–Zn alloy system is different and characterised by a series of stable Frank–Kasper phases $CaZn_5$, $CaZn_{11}$ and $CaZn_{13}$ and a large number of Ca-rich trigonal prismatic phases. A deep eutectic minimum at 75 at.% Ca leads to the depression of the melting point by 22% relative to the composition average. An amorphous phase is formed in the range 40–80 at.% Ca. Hafner and Tegze (1989) made a detailed molecular dynamic study of the atomic structure of liquid and amorphous Ca–Zn alloys, based on interatomic forces derived from optimised first-principles pseudopotentials. They concluded that the liquid and the quench-condensed amorphous phase can be described as being disordered tetrahedrally close packed with the trigonal prismatic local order in analogy with the trigonal prismatic structures of the crystalline counterpart. They predicted the occurrence of the prepeak in the partial structure factor $S_{Zn\text{-}Zn}(Q)$ as a result of the topological short-range order.

The electronic structure of Ca–Al, Ca–Mg and Ca–Zn amorphous alloys has been calculated, using the realistic model for the atomic structure derived from the first-principle interatomic potentials mentioned above (Hafner and Jaswal 1988, Jaswal and Hafner 1988, Tegze and Hafner 1989). It is found that the Ca 3d states occupy a sizable proportion of the density of states at E_F in all these alloy systems. A striking difference in the electron transport properties was rather attributed to the different degrees of s- and p-electron dehybridisation. The valence band in the Ca–Al alloys is essentially split into two; one part occupied exclusively by Al 3s states at higher binding energies and the other by the Al 3p states hybridised with the Ca 4s, 4p and 3d states at lower binding energies. The corresponding dehybridisation in the Ca–Mg is weak and, hence, complete splitting does not occur. The splitting in the Ca–Zn amorphous alloys is predicted to occur with a degree intermediate between Ca–Mg and Ca–Al. The isolation of the Al 3s states from the valence band in Ca–Al is due to the large energy difference of about 5 eV between the atomic Al 3s and Ca 4s levels, which is much larger than the differences of 1.5 and 3 eV for the Mg 3s/Ca 4s and Zn 4s/Ca 4s atomic levels, respectively (Herman and Skillman 1963, Hafner and Jaswal 1988).

We consider it timely, therefore, to study experimentally the atomic and electronic structure and the electron transport properties of Ca–Zn amorphous

Table 1. Low-temperature specific heat data for Ca_xZn_{100-x} amorphous alloys. The value of γ_{band} has been calculated by Hafner and Tegze (1990).

x	γ (mJ mol^{-1} K^{-2})	α (mJ mol^{-1} K^{-4})	δ (mJ mol^{-1} K^{-6})	Θ_D (K)	γ_{band} (mJ mol^{-1} K^{-2})
			Amorphous		
17	—	—	—	—	1.11
33	—	—	—	—	1.34
45	1.73 ± 0.02	0.225 ± 0.002	0.0010	205.1 ± 0.5	—
50	1.80 ± 0.02	0.222 ± 0.002	0.0006	206.0 ± 0.5	1.91
64	2.17 ± 0.02	0.261 ± 0.003	0.0015	195.2 ± 0.7	—
75	2.28 ± 0.02	0.252 ± 0.002	0.0011	197.7 ± 0.5	2.55
			Crystalline		
17 ($CaZn_5$)	1.09 ± 0.01	0.058 ± 0.001	−0.0001	322.3 ± 1.1	0.78
33 ($CaZn_2$)	1.57 ± 0.01	0.094 ± 0.001	−0.0001	274.6 ± 0.7	0.94
50 (CaZn)	2.38 ± 0.01	0.137 ± 0.001	—	241.9 ± 0.1	1.91
75 (Ca_3Zn)	3.24 ± 0.01	0.188 ± 0.001	0.0008	217.9 ± 0.4	2.71

alloys and to compare the results with the theoretical predictions by Hafner and his colleagues and also with the experimental data available for the Ca–Al, Ca–Mg and other sp-electron amorphous alloys.

2. Experimental procedure and results

The Ca_xZn_{100-x} (x = 17, 33, 45, 50, 64 and 75) ingots were prepared by melting the components (99.5% Ca and 99.999% Zn) in an induction furnace in an Ar gas atmosphere of almost 760 Torr. Ribbon samples were fabricated by the melt-spinning technique in the reduced Ar gas atmosphere. The formation of an amorphous single phase was confirmed by x-ray diffraction with Cu Kα radiation for the alloys with x = 45–75. A prepeak in the amorphous phase was searched for, using Cu Kα radiation (20 mA, 40 kV) with a step-scanning mode of $2\theta = 0.05°$ for 30 s of data accumulation in each step. It took about 12.5 h to cover the 2θ range 5–80°. N_2 gas was blown against the surface of the ribbon sample to minimise the oxidation during the measurements. The crystalline intermetallic compounds $CaZn_5$, $CaZn_2$, CaZn and Ca_3Zn were prepared by annealing the ingot sealed in a glass tube under an Ar gas atmosphere in the temperature range 650–670 K for more than a week.

The low-temperature specific heats were measured in the range 1.5–6 K using the adiabatic method. A mass of typically 1.5–2 g was used for the measurements. The electrical resistivity was measured by a conventional four-probe DC method in the range between 2 and 300 K. The magnetic susceptibility was determined at room temperature, using the ordinary Faraday balance under a magnetic field of 4.4–14 kOe. The Hall coefficient was measured by the five-probe DC method in the range 77–300 K. The integration method was employed for the thermoelectric power measurement in the temperature range 77–570 K. The liquid nitrogen was used as a cold reservoir. A mass density was also measured at room temperature using Archimedes' method with toluene as the working fluid. The x-ray photoemission valence band spectra were measured,

using an x-ray source with a monochromatised Al Kα line (Surface Science Instruments, SSX-100).

Numerical data for the low-temperature specific heats and the other relevant data are summarised in tables 1 and 2, respectively.

3. Discussion

3.1. Atomic structure

The local atomic structure of the Ca-rich amorphous alloys has been described in terms of the trigonal prismatic unit in analogy with the corresponding crystalline intermetallic compounds Ca_3Zn (Re_3B type), Ca_5Zn_3 (Cr_5B_3 type) and CaZn (CrB type) (Hafner and Tegze 1989). They predicted the occurrence of a prepeak in the partial structure factor $S_{Zn-Zn}(Q)$ and the number-density structure factor $S_{NN}(Q)$ as a result of this unique local order in Ca-rich amorphous alloys. Figure 1 reproduces the composite x-ray structure factor for the $Ca_{75}Zn_{25}$ amorphous alloy calculated by Hafner and Tegze (1990). It shows the prepeak at about 1.25 $Å^{-1}$. The measured x-ray diffraction data for the $Ca_{75}Zn_{25}$ amorphous alloy is incorporated in figure 1 after subtracting the background contribution. A prepeak is clearly found at the same scattering wavenumber. Although an attempt has been extended to other Ca-based amorphous alloys, unavoidably rapid oxidation during measurements prevented us from detecting its presence. Nevertheless, we believe that the experimental confirmation of the presence of a prepeak in the $Ca_{75}Zn_{25}$ amorphous alloy is strong enough to validate their self-consistent atomic and electronic structure calculations and for us to proceed with our discussion on the electronic structure and the electron transport properties by utilising their band calculations as a useful guide.

3.2. Electronic structure

Figure 2 shows the total and partial density of states calculated by Tegze and Hafner (1989) for the amorphous $Ca_{50}Zn_{50}$ alloy. It is clear that the Ca 3d, Ca 4p and Zn 4p states dominate at E_F, while the Zn 4s states are found well below E_F. The Zn 4s states are centred at about 3 eV below E_F, resulting in a dip in the total density-of-states curve. Figure 3 shows the experimentally derived x-ray photoemission spectroscopy (XPS) valence band structure for the amorphous $Ca_{50}Zn_{50}$ alloy in comparison with the XPS profile calculated by Hafner and Tegze (1990). First of all, a sharp peak observed near the bottom of the XPS valence band spectrum can be easily identified as the Zn 3d band. The measured Zn 3d band is centred at a binding energy of 9.4 eV and is about 2 eV higher than the calculated band centred at about 7.4 eV. Such d-band shift is generally observed regardless of the atomic structure and attributed to the self-energy effect (Hafner *et al* 1988).

The observed XPS profile above the Zn 3d band is apparently similar to the calculated XPS spectrum. A decreasing slope with a subsequent dip in the calculated XPS spectrum reflects well the feature of the total density of states shown in figure 2. It should be noted that the hump at the binding energy of about 6 eV in the measured XPS spectrum is caused by the O 2p states associated with oxygen contamination. In spite of this unfavourable superposition of the extra peak, we consider that the measured XPS valence band spectrum well exhibits features characteristic of the calculated band structures.

Table 2. Electronic properties of Ca_xZn_{100-x} amorphous alloys. TCR is the temperature coefficient of resistivity. DSC refers to the differential scanning calorimetry measurements. The ionic magnetic susceptibility χ_{ion} is calculated using the data for $\chi_{ion}(Ca^{2+}) = -10.42 \times 10^{-6}$ emu mol^{-1} and $\chi_{ion}(Zn^{2+}) = -11.45 \times 10^{-6}$ emu mol^{-1} in the literature (Mizutani and Matsuda 1983).

x	ρ_{300K} ($\mu\Omega$ cm)	ρ–T type	TCR (10^{-4} K^{-1})	R_H (10^{-11} m^3 A^{-1} s^{-1})	d (g cm^{-3})	$(e/a)_{eff}$	S_{300K} (μV K^{-1})	T_x (K) DSC	T_x (K) S	T_x (K) Resistivity	χ_{exp} (10^{-5} emu mol^{-1})	χ_{ion} emu mol^{-1})
45	119 ± 1	b	−0.646	−7.7 ± 0.2	3.82	1.91	3.7	422	410	411	1.98	−1.10
50	112 ± 3	b	−0.246	−8.5 ± 0.1	3.56	1.81	3.6	418	408	412	2.17	−1.09
64	95 ± 1	a	0.303	−11.5 ± 0.4	2.47	1.80	3.0	402	396	390	2.74	−1.08
75	71 ± 4	a	1.05	−16.1 ± 0.2	1.57	1.91	2.4	397	386	384	3.16	−1.07

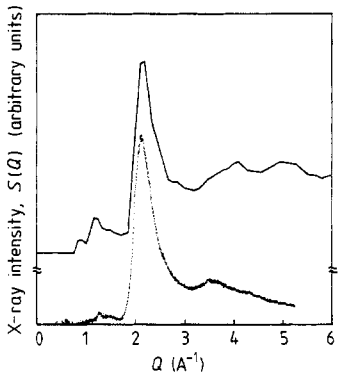

Figure 1. The x-ray diffraction spectrum measured with the step-scanning mode for $Ca_{75}Zn_{25}$ amorphous alloy. The composite structure factor $S(Q)$ calculated by Hafner and Tegze (1990) (——) is included.

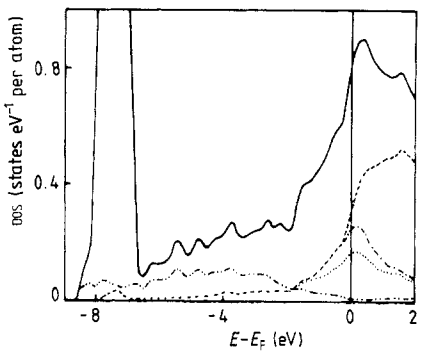

Figure 2. Total and partial density of states for $Ca_{50}Zn_{50}$ amorphous alloy calculated by Tegze and Hafner (1989). The Fermi level is taken as an origin of the energy axis. A large peak in the binding energy below 7 eV represents the Zn 3d band. Partial density of states are as follows: – – –, Ca 3d; —·—, Ca 4p; —··—, Zn 4s; ·····, Zn 4p.

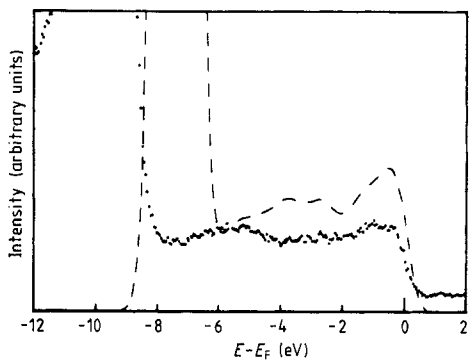

Figure 3. XPS valence band spectrum obtained using the Al Kα (1486 eV) line. The calculated XPS valence band spectrum (– – –) by Hafner and Tegze (1990) for amorphous $Ca_{50}Zn_{50}$ alloy is included. The Fermi level is taken as the origin of the energy axis.

The XPS spectra were also taken for Ca–Zn amorphous alloys with different Ca contents. The general features are essentially the same except for the gradual growth of the width of the Zn 3d band with decreasing Ca content. The XPS valence band spectra were also measured for the CaZn intermetallic compound, but we could not differentiate between these spectra and those from the corresponding amorphous alloy within the resolution of the measurements. This is reasonable, since the calculated density-of-states curve for the crystalline state resembles that in the amorphous state except for the presence of the fine structures (Tegze and Hafner 1989).

Figure 4(a) shows the Ca concentration dependence of the electronic specific heat coefficient γ in the amorphous Ca–Zn alloys, along with the data for the amorphous Ca–Mg, Ca–Al and Ca–Cu alloys (Mizutani and Matsuda 1983, Mizutani *et al* 1987a, Mizutani *et al* 1988b). Correspondingly, the calculated values are shown in figure 4(b) (Hafner and Jaswal 1988, Jaswal and Hafner 1988, Hafner and Tegze 1990). The value of γ in all Ca-based amorphous alloys is distributed over 1.6–2.4 mJ mol^{-1} K^{-2} and is

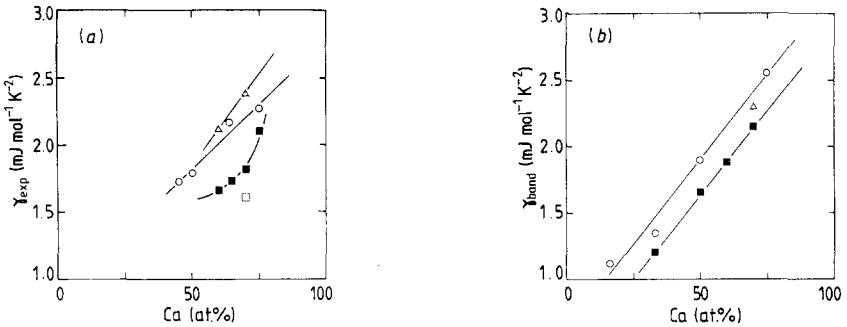

Figure 4. (*a*) The measured electronic specific heat coefficient γ_{exp} and (*b*) and γ_{band} calculated by Hafner and Tegze (1990) as a function of Ca content for Ca-based amorphous alloys: ○, Ca–Zn (present results, Hafner and Tegze 1989); ■, Ca–Al (Mizutani and Matsuda 1983); △, Ca–Mg (Mizutani *et al* 1987a); □, Ca–Cu (Mizutani *et al* 1988b).

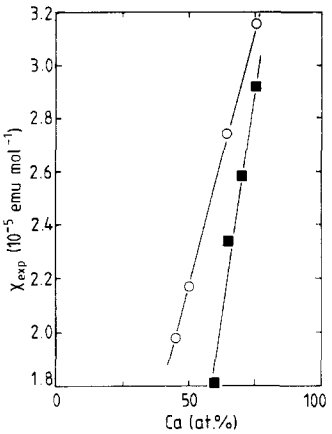

Figure 5. Measured magnetic susceptibility at 300 K as a function of Ca content for the Ca-based amorphous alloys: ○, Ca–Zn (present results); ■, Ca–Al (Mizutani and Matsuda 1983).

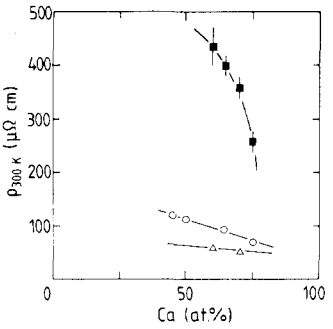

Figure 6. The electrical resistivity at 300 K as a function of Ca content for Ca-based amorphous alloys; ○, Ca–Zn (present results); ■, Ca–Al (Mizutani and Matsuda 1983); △, Ca–Mg (Mizutani *et al* 1987a).

rather high relative to those found in other sp-electron amorphous alloys based on Al, Mg and noble metals (Mizutani and Yoshino 1984, Mizutani *et al* 1990). Both experimental and theoretical values of γ are found to agree with each other and to decrease rapidly with decreasing Ca concentration, regardless of the atomic species of the partner elements Mg, Al and Zn. It can also be seen that the measured value of γ in Ca–Zn is consistently lower than that in Ca–Mg but is higher than in Ca–Al, but the difference is not substantial. As listed in table 1, the low-temperature specific heats were also measured for the Ca–Zn intermetallic compounds. The value of γ for the compounds is also found to decrease with decreasing Ca content in good agreement with the values calculated by Hafner and Tegze (1990).

Figure 5 shows the Ca concentration dependence of the magnetic susceptibility for the present Ca–Zn amorphous alloys, along with the previous data for the Ca–Al

amorphous alloys (Mizutani and Matsuda 1983). It increases sharply with increasing Ca content in both alloy systems, the general trend being consistent with the behaviour of the electronic specific heat coefficient. Emphasis may be placed on the fact that the observed paramagnetism is fairly large compared with those of other sp–electron amorphous alloys, suggesting that the Ca 3d states at E_F contribute not only to enhancing the Pauli paramagnetism but also to inducing the van Vleck orbital paramagnetism (Mizutani and Matsuda 1983).

From all these experimental results, we conclude that the densities of states at E_F are similar for all Ca–X (X ≡ Mg, Al, Zn and Cu) amorphous alloys and are characterised by the enhancement due to the hybridisation of the Ca 3d and Ca 4p states with the p states of the partner element X.

3.3. Electron transport properties

Figure 6 shows the Ca concentration dependence of the electrical resistivity at 300 K for amorphous Ca–Zn alloys, together with those for Ca–Mg and Ca–Al alloys (Mizutani and Matsuda 1983, Mizutani *et al* 1987a), The resistivity of Ca–Zn alloys is distributed over the range 70–120 $\mu\Omega$ cm and falls in between those of Ca–Al and Ca–Mg. Moreover, the value is found to decrease with increasing Ca content, irrespective of the partner elements Mg, Zn and Al.

The ρ–T data below 300 K are depicted in figure 7 for amorphous Ca–Zn alloys. For comparison, the data for Ca–Mg–Al alloys are reproduced in its inset (Mizutani *et al* 1987a). It has been claimed that the temperature dependence of the electrical resistivity below 300 K in non-magnetic amorphous alloys can be classified in terms of five different types a–e, which appear in the alphabetical sequence with increasing resistivity in a given alloy system (Mizutani 1988, Mizutani *et al* 1990). As can be seen from the inset, the ρ–T types change from a to d successively with increasing Al content or increasing resistivity in the Ca–Mg–Al system. Note here that the resistivity increases from 40 to about 400 $\mu\Omega$ cm upon substituting Al for Mg. In contrast, one can see only a gradual change in the ρ–T types from a to b in the amorphous Ca–Zn alloys. This is quite reasonable, since the resistivity varies only in the limited range as mentioned above. It may be noted that the resistivity maximum temperature T_{max} decreases with increasing Zn content or increasing resistivity. The value of T_{max} is plotted in figure 8 as a function of resistivity for not only Ca-based amorphous alloys but also for other sp-electron amorphous alloys, in all of which the ρ–T relationship is type b. It can be seen that the T_{max} vanishes at about 200 $\mu\Omega$ cm in all Ca-based alloys, indicating that the type b terminates and switches to type c at this resistivity. This critical resistivity is fairly high compared with the corresponding value of about 90 $\mu\Omega$ cm observed for the Mg-based amorphous alloys (Mizutani *et al* 1987a). We emphasised in the preceding section that the number of Ca 3d states is large at the Fermi level in all Ca-based amorphous alloys. Nevertheless, we found that the observed ρ–T types and their successive change with increasing resistivity are consistent with what has been observed in typical sp-electron amorphous alloys and, hence, behave as if no d electrons exist at E_F.

Figure 9(*a*) illustrates the interrelation between the resistivity at 300 K and the electronic specific heat coefficient, which is a measure of the density of states at E_F, for a large number of non-magnetic amorphous alloys including the Ca-based alloys. They are essentially grouped into three families. The first is denoted as the d-electron system and refers to alloys, in which the d-electron dominates the density of states at E_F. Examples are Cu–Zr–Al (Mizutani *et al* 1987b) and Ni–Zr–X (X ≡ B, Si, Al) (Yamada

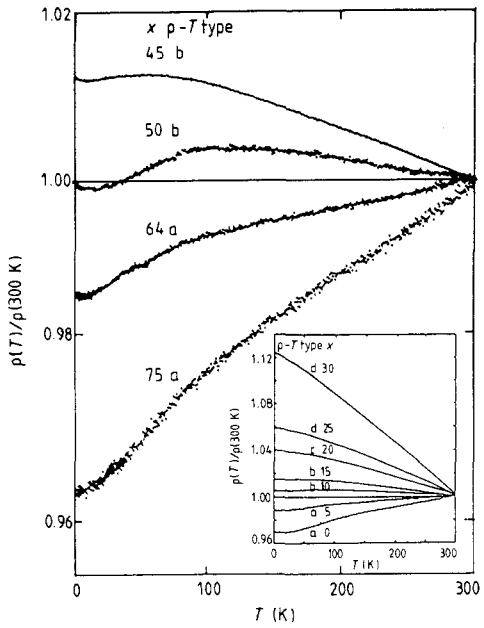

Figure 7. The temperature dependence of the electrical resistivity normalised with the value at 300 K for the Ca_xZn_{100-x} amorphous alloys. The ρ–T types are indicated by roman lower-case letters. The inset shows the data for the $Ca_{70}Mg_{30-x}Al_x$ amorphous alloys (Mizutani *et al* 1987a).

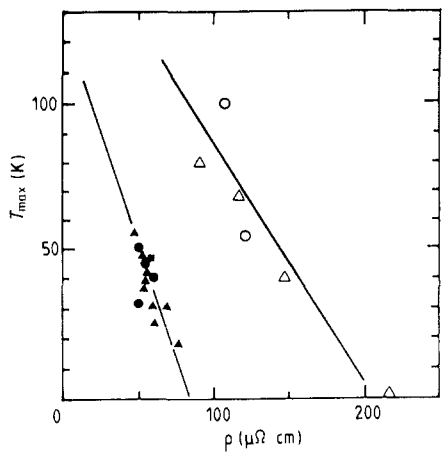

Figure 8. The resistivity maximum temperature T_{max} as a function of resistivity at 300 K: ○, Ca–Zn (present results); △, Ca–Mg–Al (Mizutani *et al* 1987a); ▲, ●, other Mg-based amorphous alloys (Mizutani *et al* 1987a).

et al 1987). The second family is denoted as the sp-electron system and includes Mg–Zn–Ga (Matsuda *et al* 1984), Al–Ni–X (X ≡ Si, Ge, etc) (Mizutani *et al* 1990) and Ag–Cu–X (X ≡ Mg, Si and Ge) (Mizutani and Yoshino 1984). Here the d-electron contribution to electron transport is absent. The last family is the Ca-based alloys, which are intermediate regarding the degree of the occupation of the d electrons at E_F. The difference in the electronic structure is indeed well reflected in the plot of ρ versus γ shown in figure 9(*a*).

An apparent consistency with the generalised Faber–Ziman theory for the Ca-based alloys with types a–c suggests that the sp electrons are mostly responsible for elecron conduction in spite of the presence of the discernible d electrons at the Fermi level. In addition, judging from the band-structure calculations by Tegze and Hafner (1989), we tend to believe that the Zn 4p and Ca 4p electrons are largely responsible for electron conduction and that they possess a mean free path longer than the average atomic distance in the low-resistivity regime characterised by types a and b. Indeed, all Ca–Zn amorphous alloys studied in this experiment belong to this regime.

To shed more light on the Ca-based amorphous alloys, we plotted the relevant data on an expanded scale in figure 9(*b*). The ρ–T types are also shown. It can be seen that the curve drawn through the data points in the respective alloy systems becomes steeper in the sequence Mg, Zn and Al. The higher the resistivity, the more substantially a reduction in γ enhances the resistivity. Remember that the reduction in γ with decreasing

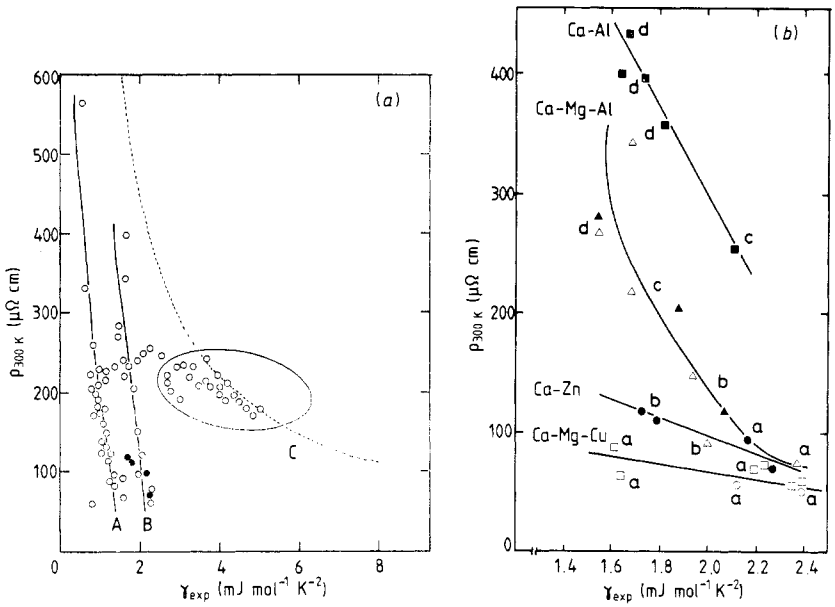

Figure 9. (*a*) The resistivity at 300 K as a function of the measured electronic specific heat coefficient γ_{exp} for a large number of non-magnetic amorphous alloys: the broken curve shows the possible high-resistivity limiting envelope (Mizutani *et al* 1990). Curve A is drawn through the data points for Mg-, Al- and noble metal-based sp-electron amorphous alloys, whereas curve B is drawn through the data points for Ca-based alloys. The data encircled and denoted as curve C represent those for d-electron systems. (*b*) The blow-up of (*a*) for the Ca-based amorphous alloys. The ρ–T types are marked by roman lower-case letters.

Ca content is due to the decrease in the Ca 3d and Ca 4p states at the Fermi level. This would naturally explain a general increase in resistivity with decreasing Ca concentration in each system. The unique difference in the magnitude of the resistivity in the three relevant systems Ca–X (X ≡ Mg, Zn and Al) may be caused by the different degrees of the splitting of the Mg 3s, Zn 4s and Al 3s states from the conduction band, as predicted by Hafner and his coworkers. We shall discuss this a little further in the next section.

3.4. Hall coefficient

The Hall coefficient has been measured in the temperature range 77–300 K for amorphous Ca–Zn alloys. As shown in figure 10, the temperature dependence is almost negligible. The effective electron concentration $(e/a)_{eff}$ is calculated, using the expression

$$(e/a)_{eff} = 1.036 \times 10^{-11} A/d(-R_H) \tag{1}$$

where A is the average atomic weight in grams, d is the measured density in grams per cubic centimetre and R_H is the measured Hall coefficient in cubic metres per ampere second. The value of $(e/a)_{eff}$ is plotted in figure 11 as a function of Ca concentration for all Ca-based binary alloys. It can be seen that the value is close to 2 for divalent Ca–Mg and slightly less than 2 for Ca–Zn, suggesting that both Ca and the partner elements Mg and Zn donate almost two electrons per atom to the conduction band. In contrast, the value of $(e/a)_{eff}$ in Ca–Al is extremely small. Hafner and Jaswal (1988) suggested that

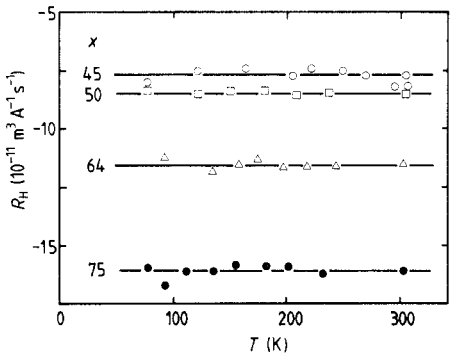

Figure 10. The Hall coefficient as a function of temperature for the Ca_xZn_{100-x} amorphous alloys.

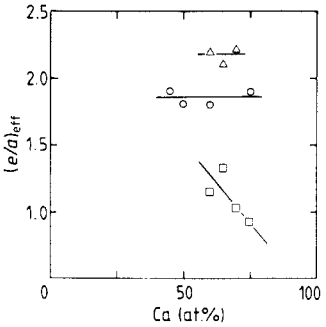

Figure 11. The effective electron concentration calculated from equation (1) against the Ca content for Ca-based amorphous alloys: ○, Ca–Zn (present results); □. Ca–Al (Mizutani and Matsuda 1983); △, Ca–Mg (Mizutani *et al* 1987a).

this reduction results from the complete separation of the low-lying Al 3s states from the conduction band. We would then expect a decrease in $(e/a)_{\text{eff}}$ with increasing resistivity or decreasing Ca concentration, particularly in the Ca–Al alloy system. However, the results in figure 11 are not consistent with this simple picture. The reason for this is not clear at this moment.

3.5. Thermoelectric power

The thermoelectric power for the amorphous Ca–Zn alloys is plotted in figure 12 in the temperature range 77–570 K. It is positive over the whole temperature range and changes abruptly upon crystallisation. The crystallisation temperature thus obtained agrees well with those deduced from the high-temperature resistivity and DSC measurements, which will be discussed in the next section.

It is of great interest to examine what parameters are critically important in deciding the magnitude of the thermoelectric power $S_{300\,\text{K}}$ at 300 K in non-magnetic amorphous alloys, where the electron–phonon enhancement effect may be less important (Sato *et al* 1987). Various attempts have so far been made to correlate the value of $S_{300\,\text{K}}$ with

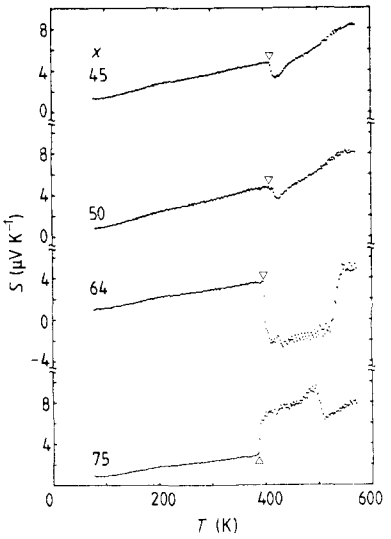

Figure 12. The thermoelectric power as a function of temperature for the Ca_xZn_{100-x} amorphous alloys: △, ▽, onset of crystallisation.

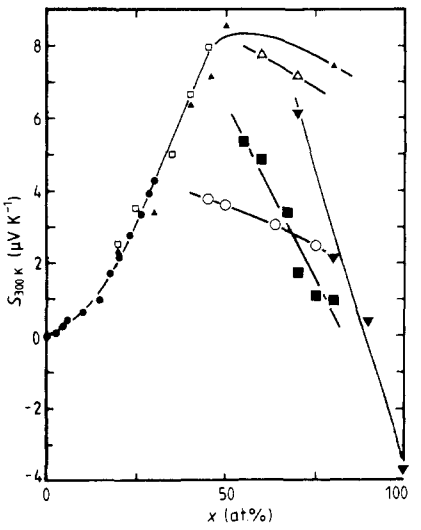

Figure 13. The thermoelectric power at 300 K as a function of total content of Cu, Ag and Ca for Mg- and Ca-based amorphous alloys: ●, $Mg_{70}Zn_{30-x}Cu_x$ (Mizutani and Matsuda 1987); □, $Mg_{100-x}Cu_x$ (Matsuda *et al* 1986); ▲, Ag–Cu–Mg (Matsuda *et al* 1986); △, Ca–Mg (Mizutani and Matsuda 1985); ■, Ca–Al (Naugle *et al* 1986); ▼, $Ca_{70}Mg_{30-x}Cu_x$ (Mizutani *et al* 1988b); ○, Ca–Zn (present data).

other physical quantities such as the resistivity (Kaiser 1987) and the Hall coefficient (Harris 1986). However, the detailed analysis, using the data for a large number of typical sp-electron amorphous alloys, failed to find any correlations with these physical quantities (Mizutani and Matsuda 1987).

In order to extract a common feature as systematically as possible, we collected the value of $S_{300\,K}$ for not only the present Ca–Zn amorphous alloys but also other Ca- and Mg-based amorphous alloys so far studied. The data for the amorphous Ca–Mg (Mizutani and Matsuda 1985), Ca–Al (Naugle *et al* 1986), $Ca_{70}Mg_{30-x}Cu_x$ (Mizutani *et al* 1988b), $Mg_{90}Zn_{30-x}Cu_x$ (Mizutani and Matsuda 1987), $Mg_{100-x}Cu_x$, $Mg_{100-x}Ag_xCu_{3x}$ and $Mg_{100-x}Ag_xCu_x$ (Matsuda *et al* 1986) are included. The value of $S_{300\,K}$ is plotted in figure 13 against the total content of Cu, Ag and Ca, all of which introduce d states near the Fermi level when dissolved in the amorphous matrix.

An interesting correlation clearly emerges, particularly for the Mg-based amorphous alloys containing Cu and/or Ag. The value of $S_{300\,K}$ falls well on a universal curve and increases with increasing Cu plus Ag content up to about 50 at.% and then decreases slowly beyond this concentration. Note that the value of $S_{300\,K}$ for $Mg_{70}Zn_{30-x}Ga_x$ remains essentially zero with increasing Ga concentration (Matsuda *et al* 1984). Hence, we tend to believe that the d states of Cu and Ag somehow play a critical role in determining the magnitude of the thermoelectric power.

The data for Ca-based amorphous alloys are less universal on this scale. However, the value of $S_{300\,K}$ decreases with increasing total content of Ca and Cu without exception

and, furthermore, the data for the $Ca_{70}Mg_{30-x}Cu_x$ alloys are apparently fitted to this general trend up to the $Ca_{70}Cu_{30}$ alloy, which takes a negative value at the very end of the composition axis. As discussed in the preceding section, the Ca 3d states dominate at the Fermi level in all Ca-based amorphous alloys. Hence, the role of the d states is again suggested to be of crucial importance.

Figure 13 also suggests that the value of S_{300K} for the Ca-based amorphous alloys would decrease with decreasing Ca content below 50 at.% in a manner similar to that for the Mg-based amorphous alloys. It is, therefore, of great interest to measure the thermoelectric power in the Ca-poor composition range and, in particular, to study the effect of the addition of Ca atoms to the Mg–Zn amorphous alloy, since it is thermoelectrically a zero alloy and is ideally suited to determining the effect of the third element on the thermoelectric power.

3.6. Crystallisation temperature

The presence of an interrelationship between the crystallisation temperature T_x and the Debye temperature Θ_D for non-magnetic amorphous alloys has been pointed out and discussed in relation to the Lindemann melting law (Mizutani *et al*1990). The T_x–Θ_D plots are well divided into d-electron and sp-electron systems and fitted to two respective straight lines. The data for the d-electron system always has a higher crystallisation temperature than those for the sp-electron system at a given Debye temperature. The crystallisation temperature has been determined in this experiment from three independent measurements: resistivity, thermoelectric power and DSC measurements with heating rates of 10, 2.5 and 10 K min^{-1}. The resistivity data are shown in figure 14. The value of T_x thus derived is correlated with the Debye temperature listed in table 1 and compared with the data in the literature (Mizutani *et al* 1990). It is found that the Ca-based amorphous alloys can be regarded as a typical sp-electron system in terms of the T_x–Θ_D plot in spite of the possession of a noticeable amount of d electrons at the Fermi level.

4. Conclusion

The valence band structure and the electron transport properties for the Ca–Zn amorphous alloys have been experimentally studied and discussed in comparison with the band-structure calculations due to Hafner and Tegze and with the experimental data available for other Ca- and Mg-based amorphous alloys. Both x-ray photoemission and the electronic specific heat measurements confirmed that the density of states at the Fermi level is enhanced by the presence of the Ca 3d states. We found that, in spite of the possession of the measurable amount of Ca 3d states at the Fermi level, the electron transport properties and the crystallisation temperature behave in a manner consistent with those observed for Ag–Cu–X (X ≡ Mg, Al, Ge, etc), Al-rich Al–Ni–X (X ≡ Ti, Zr, La) and Mg–Zn–X (X ≡ Ga, Sn) amorphous alloys, in which only sp electrons dominate at the Fermi level.

Acknowledgments

We are most grateful to Professor J Hafner, Technische Universität Wien, for stimulating discussions and valuable comments and for allowing us to refer to his theoretical results

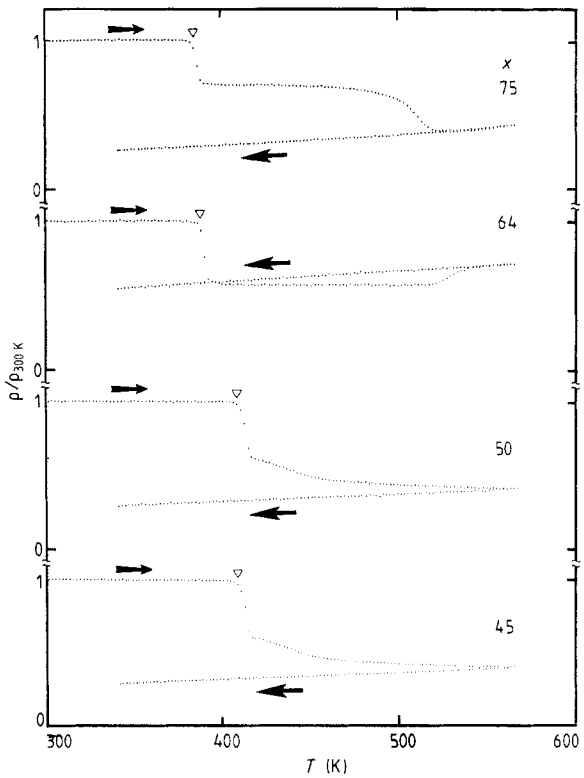

Figure 14. The resistivity as a function of temperature above 300 K for Ca_xZn_{100-x} amorphous alloys: ▽, onset of crystallisation.

concerning XPS spectra, the values of γ and composite structure factors prior to publication. We also wish to acknowledge fruitful discussions with Professor H Sato, Aichi University of Education. We also thank K Hosoda, K Nakamura and Y Hoshino for the assistance with the sample preparation and the measurements of various electronic properties.

References

Hafner J and Jaswal S S 1988 *Phys. Rev.* B **38** 7320
Hafner J, Jaswal S S, Tegze M, Pflugi A, Krieg J, Oelhafen P and Güntherodt H-J 1988 *J. Phys. F: Met. Phys.* **18** 2583
Hafner J and Tegze M 1989 *J. Phys.: Condens. Matter* **1** 8277
—— 1990 to be published
Harris R 1986 *J. Phys. F: Met. Phys.* **16** 53
Herman F and Skillman S 1963 *Atomic Structure Calculations* (Englewood Cliffs, NJ: Prentice-Hall)
Howson M A, Hickey B J and Morgan G J 1988 *Phys. Rev.* B **38** 5267
Jaswal S S and Hafner J 1988 *Phys. Rev.* B **38** 7311
Kaiser A B 1987 *Phys. Rev.* B **35** 2480
Matsuda T, Mizutani U and Sato H 1986 *J. Phys. F: Met. Phys.* **16** 1005
Matsuda T, Shiotani N and Mizutani U 1984 *J. Phys. F: Met. Phys.* **14** 1193
Mizutani U 1988 *Mater. Sci. Eng.* **99** 165

Mizutani U and Matsuda T 1983 *J. Phys. F: Met. Phys.* **13** 2115
—— 1985 *Proc. 4th Int. Conf. on Rapidly Quenched Metals* ed S Steeb and H Warlimont (Amsterdam: North-Holland) p 1035
—— 1987 *J. Non-Cryst. Solids* **94** 345
Mizutani U, Ohashi S, Matsuda T, Fukamichi K and Tanaka K 1990 *J. Phys.: Condens. Matter* **2** 541
Mizutani U, Sasaura M, Moruzzi V L and Matsuda T 1988b *Mater. Sci. Eng.* **99** 295
Mizutani U, Sasaura M, Yamada Y and Matsuda T 1987a *J. Phys. F: Met. Phys.* **17** 667
Mizutani U, Sato K, Sakamoto I and Yonemitsu K 1988a *J. Phys. F: Met. Phys.* **18** 1995
Mizutani U, Yamada Y, Mishima C and Matsuda T 1987b *Solid State Commun.* **62** 641
Mizutani U and Yoshino K 1984 *J. Phys. F: Met. Phys.* **14** 1179
Nagel S R, Gubler U M, Hague C F, Krieg J, Lapka R, Oelhafen P, Güntherodt H-J, Evers J, Weiss A, Moruzzi V L and Williams A R 1982 *Phys. Rev. Lett.* **49** 575
Naugle D G, Delgado R, Armbrüster H, Tsai C L, Callaway T O, Reynolds D and Moruzzi V L 1986 *Phys. Rev.* B **34** 8279
Sato H, Matsuda T and Mizutani U 1987 *Physica* B **144** 173
Tegze M and Hafner J 1989 *J. Phys.: Condens. Matter* **1** 8293
Tsai C L, Hong J and Giessen 1982 *Proc. 4th Int. Conf. on Rapidly Quenched Metals* vol 2, ed T Masumoto and K Suzuki (Sendai: Japan Institute of Metals) pp 1327–30
Yamada Y, Itoh Y, Matsuda T and Mizutani U 1987 *J. Phys. F: Met. Phys.* **17** 2313